ELSEVIER

Contents lists available at ScienceDirect

## Science of the Total Environment

journal homepage: www.elsevier.com/locate/scitotenv



# Identifying snowfall elevation patterns by assimilating satellite-based snow depth retrievals



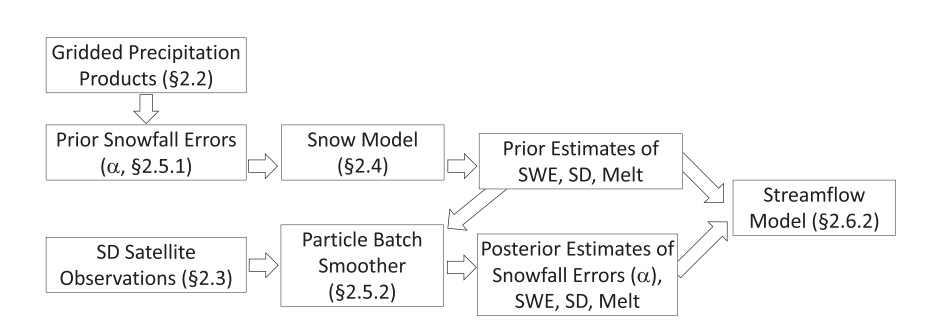
Manuela Girotto <sup>a,\*</sup>, Giuseppe Formetta <sup>b</sup>, Shima Azimi <sup>b</sup>, Claire Bachand <sup>a,c</sup>, Marianne Cowherd <sup>a</sup>, Gabrielle De Lannoy <sup>d</sup>, Hans Lievens <sup>d,e</sup>, Sara Modanesi <sup>f</sup>, Mark S. Raleigh <sup>g</sup>, Riccardo Rigon <sup>b</sup>, Christian Massari <sup>f</sup>

- <sup>a</sup> Environmental Science and Policy Management, University of California, Berkeley, CA, USA
- <sup>b</sup> Department of Civil, Environmental and Mechanical Engineering, University of Trento, Trento, Italy
- <sup>c</sup> Los Alamos National Laboratory, Los Alamos, USA
- <sup>d</sup> Soil and Water Management, Katholieke Universiteit Leuven, Leuven, Belgium
- <sup>e</sup> Department of Environment, Ghent University, Ghent, Belgium
- f Research Institute for Geo-Hydrological Protection, National Research Council, Perugia, Italy
- g College of Earth, Ocean, and Atmospheric Sciences, Oregon State University, OR, USA

#### HIGHLIGHTS

- The assimilation of Sentinel-1 snow depth identifies biases in gridded precipitation products across elevation gradients
- The posterior cumulative snowfall elevation patterns are consistent across precipitation products
- Correcting the spatial distribution of snowfall leads to basin-wide improved snow and streamflow estimates

#### G R A P H I C A L A B S T R A C T



## ARTICLE INFO

Editor: Ouyang Wei

Keywords: Mountain hydrology Snowfall correction Data assimilation Snowfall gradients Sentinel-1 Snow depth

#### ABSTRACT

Precipitation in mountain regions is highly variable and poorly measured, posing important challenges to water resource management. Traditional methods to estimate precipitation include in-situ gauges, Doppler weather radars, satellite radars and radiometers, numerical modeling and reanalysis products. Each of these methods is unable to adequately capture complex orographic precipitation. Here, we propose a novel approach to characterize orographic snowfall over mountain regions. We use a particle batch smoother to leverage satellite information from Sentinel-1 derived snow depth retrievals and to correct various gridded precipitation products. This novel approach is tested using a simple snow model for an alpine basin located in Trentino Alto Adige, Italy. We quantify the precipitation biases across the basin and found that the assimilation method (i) corrects for snowfall biases and uncertainties, (ii) leads to cumulative snowfall elevation patterns that are consistent across precipitation products, and (iii) results in overall improved basin-wide snow variables (snow depth and snow cover area) and basin streamflow estimates.

E-mail address: mgirotto@berkeley.edu (M. Girotto).

<sup>\*</sup> Corresponding author.

#### 1. Introduction

Mountain head-watersheds are often referred to as "water towers" because they store freshwater during winter months and release it when it is most needed for agriculture purposes during the spring and summer months (e.g., Viviroli et al., 2007; Immerzeel et al., 2020; Qin et al., 2020). The hydrology of mountains is driven by orographic (i.e., elevation dependent) precipitation, an inherently complex physical mechanism that brings enhanced amounts of rain and snow to the higher elevations of the mountains (e.g., Mott et al., 2014; Sarmadi et al., 2019). The mechanism is poorly understood because of the complicated feedbacks between the complex terrain and the atmosphere. The knowledge uncertainty in snowfall spatial patterns primarily encompasses magnitude and seasonality of precipitation elevation gradients, as well as the drivers (e.g., landscape or atmospheric variables) of their variability (Harpold et al., 2017; Avanzi et al., 2020).

The knowledge gap around the spatiotemporal heterogeneity of orographic precipitation is exacerbated by the lack of reliable precipitation observations in mountain regions. Meteorological networks at high elevations are sparse (Bhatt and Nakamura, 2005) and, in snowdominated regions, precipitation gauges are prone to large errors because of wind-driven undercatch or snow plugging issues (Rasmussen et al., 2012). Radar- or satellite-based observations or retrievals in mountain terrain are challenged by complex topography, radar beam shielding, and ground echoing (Germann et al., 2006). The lack of in-situ precipitation or radar- and satellite-based observations caused several regional and global mountain hydrology studies to rely on readily and globally available precipitation products that come from satellite (e.g., Global Precipitation Measurement, GPM Huffman et al., 2018), reanalysis sources (e.g., Modern-Era Retrospective analysis for Research and Applications, Version 2, MERRA-2 and the European centre for mediumrange weather forecasts Atmospheric Reanalysis version 5, ERA-5 Gelaro et al., 2017; Hersbach et al., 2020) and hybrid approaches (Beck et al., 2019).

Reanalysis or satellite-based precipitation products are widely available worldwide. However, these gridded precipitation products have relatively coarse resolution (i.e., >=10 km) with respect to the features of mountainous landscapes and show sub-optimal performance across mountainous terrain especially for satellite products which suffer from precipitation retrieval issues above frozen surfaces and complex terrain (Ebert et al., 2007; Scheel et al., 2011; Liu et al., 2017; Maggioni et al., 2017; Speirs et al., 2017; Xu et al., 2017; Lundquist et al., 2019; Wang et al., 2019). Despite their coarse resolutions, reanalysis and satellite products are routinely used to force hydrological models because they are readily available globally, or perhaps the only option in absence of in-situ data. At the local scale, in-situ observations of snowfall might be less uncertain than coarse scale resolutions products, but snowfall gauges also suffer from precipitation under-catch issues where the recorded snowfall tends to be biased low with respect to actual fallen precipitation amounts. When forcing snow models with the biased precipitation, the resulting SWE or snow depth ground estimates will also be severely biased (e.g., Raleigh et al., 2015; Günther et al., 2019).

A largely unexplored solution for explaining snowfall orographic gradients is to directly analyze the snow that accumulates on the ground. This approach was used in Avanzi et al. (2020) using snow accumulation estimates from snow course observations. The latter are periodic manual measurements, generally used by water managers for forecasting, collecting snow depth and snow density estimates at regular intervals over transects of various spatial extents (Rice and Bales, 2010). The key assumption with this solution is that the observed ground snow depth or snow water equivalent (SWE, the amount of water stored in the snow pack) measurements directly correspond to snowfall accumulation (only), and are therefore able to explain orographic patterns in snowfall. While this is not a safe assumption everywhere, it is reasonable for regions with weak wind-driven snow redistribution processes and little to no intermittent snow melt events in between snowfall episodes at the

ground snow depth measurement survey. Despite potentially providing a solution for the identification of orographic snowfall patterns, snow courses data are primarily available only over few data-rich mountain regions, including the western US (Pagano et al., 2004), Switzerland (e. g., Mott et al., 2023), Norway (Skaugen et al., 2012), and Finland (Lundberg and Koivusalo, 2003). These measurements are sparse or not existent over the vast majority of the water towers of the world. For these regions, high-resolution snow depth or SWE satellite retrievals could be seen as a way to overcome the lack of in-situ data.

In spite of the absence of a dedicated snow estimation satellite mission, advances in remote sensing technology continue to revolutionize the way we monitor snow over mountain regions. As a consequence, the number of scientific efforts aimed at using remote sensing to estimate snow depth or SWE at sub-kilometer spatial resolution has increased. These encompass studies that take advantage of a simple difference of land surface elevation between snow-on and snow-off images, including snow depth retrievals from airborne Lidar scanners (e.g., Painter et al., 2016) and from stereo satellite imagery (e.g., Deschamps-Berger et al., 2020).

More recently, scientific studies have proved the ability to retrieve snow depth from the increased volumetric scattering observed by active microwave satellite (e.g., Sentinel-1 snow depth retrievals, Lievens et al. (2019, 2022); Tsang et al. (2022). Other studies have focused on using the interferometry data in which snow depth is obtained based on the microwave signal phase difference between two acquired satellite scenes (Leinss et al., 2014; Conde et al., 2019). Some studies looked at using synthetic aperture radar (SAR) data to detect the presence of wet snow (Karbou et al., 2021) and snowmelt dynamics (Marin et al., 2020). Despite these advances in microwave sensing of snow depth, limitations remain with respect to applications of these remote sensing techniques to characterizing orographic snowfall estimates (Tsang et al., 2022). These observations are only available at discrete temporal frequencies in agreement with the operational overpasses of the satellite. The sparse temporal frequencies might miss significant snow accumulation events and therefore not accurately capture the accumulation dynamics in the mountain catchments.

A potential method to overcome the remote sensing observations shortcomings is data assimilation, which leverages the information content in the observations with that of a land surface model, while minimizing their limitations due to both observations and model inherent uncertainty (Girotto et al., 2014; Margulis et al., 2015; Magnusson et al., 2017; Winstral et al., 2019; Girotto et al., 2020; Smyth et al., 2022).

In this paper, we hypothesize that the orographic snowfall patterns in mountain catchments can be identified and resolved via the assimilation of satellite-based snow depth retrievals from the C-band Sentinel-1 mission. To our knowledge no other studies exist in the literature that assimilate Sentinel-1 data to explore its feasibility in characterizing patterns in mountains orographic precipitation. We test our methods over a snow dominated watershed in the Italian Alps that is, to a first order degree representative of other global mountain watersheds dominated by similar seasonal snow accumulation and melt patterns. We assert that the proposed approach can be applicable to other snow-covered mountain regions primarily because of the general availability of Sentinel-1 snow depth retrievals (Lievens et al., 2019).

Our specific objectives are: 1) to propose a novel data assimilation method to correct precipitation bias in mountainous regions with Sentinel-1 snow depth retrievals; 2) to analyze the spatial characteristics of the snowfall orographic precipitation patterns using the updated snow data product; and 3) to evaluate if the derived snowfall orographic precipitation lead to improved mountain watershed hydrology.

## 2. Methods

Methods are illustrated in the flowchart of Fig. 1. By assimilating snow depth observations, we retrieve snowfall patterns that can be used

to improve mountain hydrological variables such as snow accumulation, snow melt, and spring and summer streamflow. We test our hypothesis over a test-bed domain located in the Italian Alps, the Aurino River Basin (Fig. 2, Section 2.1), using readily and globally available gridded precipitation products (Section 2.2). In practice, the data assimilation system presented here constrains a snow model (Section 2.4) using the observed Sentinel-1 retrievals (Section 2.3). Data assimilation is indeed a tool to bridge models and observations in order to obtain optimized estimates of the specific phenomena of interest (Girotto et al., 2020). As part of the assimilation scheme (Section 2.5), an ensemble of possible prior estimates of the snowfall biases are used to run a year-long snow model (Section 2.4) that predicts, among other variables, snow depth values. The difference between predicted snow depth estimates and those observed by the satellite (Section 2.3) are used within a particle batch smoother assimilation algorithm (Section 2.5.2) to update the spatial distribution of snowfall error coefficients, as well as other variables of interest such as snow depth, SWE, and snow melt. We subsequently obtain streamflow estimates by forcing a semi-lumped streamflow model forced with rainfall and snowmelt that is output from the snow model (Section 2.6.2).

## 2.1. Study area: the Aurino River basin

We test our methods in the Aurino River basin, located in the Adige River system in the eastern Alps, marked in Fig. 2. The basin has an area of 614 km<sup>2</sup> and an elevation range between 817 and 3485 m a.s.l. Our analysis uses a 1 km-resolution model grid, corresponding to the spatial resolution of the snow depth retrievals (Section 2.3). We used the European Digital Elevation Model, version 1.1 at 25 m resolution (https ://land.copernicus.eu/imagery-in-situ/eu-dem/eu-dem-v1.1?tab=met adata) and aggregated to 1 km resolution. The basin streamflow outlet is San Giorgio Aurino (Zaramella et al., 2019), for which streamflow data from 2015 to 2019 have been downloaded from the Autonomous Province of Bolzano (https://meteo.provincia.bz.it/stazioni-idrometr iche.asp). Precipitation and air temperature in-situ data can also be freely downloaded from https://meteo.provincia.bz.it/download-dati. asp. The average observed annual precipitation for the test basin is around 950 mm, with less precipitation in the valleys and more in the mountains (from  $\sim$ 850 mm to  $\sim$ 1300 mm, Zaramella et al. (2019)). Two monitoring sites with snow depth measurements were available at Malga Merbe (lat = 47.04°; lon = 12.12°; elev = 2006 m) and Malga Fadner (lat =  $46.92^{\circ}$ ; lon =  $11.86^{\circ}$ ; elev = 2155 m) (Fig. 2a, Table A.3). These are freely available to download from the open data portal of the Provincia Autonoma di Bolzano at https://data.civis.bz.it/it/dataset /misure-meteo-e-idrografiche.

## 2.2. Meteorological forcings

We use precipitation products derived from three sources: reanalysis (ERA-5, Hersbach et al., 2020), satellite-based (the Integrated Multisatellite Retrievals for GPM, IMERG, Huffman et al., 2018) and, in-situ

local precipitation. Air temperature data at 2 m height were collected from both ERA-5 and local in-situ thermometer data (made available by the Autonomous Province of Bolzano).

The choice of ERA-5 dataset is due to its availability and demonstrably good performance over Europe (Bandhauer et al., 2022), as well as its permissive usage license (Copernicus Climate Change Service, http s://climate.copernicus.eu/climate-reanalysis). We acquired ERA-5 data from 2015 to 2019 at a 36 km spatial resolution at a daily time step. For IMERG, we use the final run version (IMERG-FR), which integrates gauge observations. The IMERG product has a spatial resolution of  $0.1^{\circ} \times 0.1^{\circ}$  and half-hourly temporal resolution. We used a daily version of the product available via https://www.earthdata.nasa.gov. The insitu precipitation and temperature estimates are obtained from in-situ observation locations of air temperature and of precipitation (Fig. 2a). We interpolated them to a gridded product using a kriging with external drift (Garen and Marks, 2005) interpolation algorithm, which accounts for elevation information (Fig. 2c and f). For mountain regions, such as the one investigated in this study, we expect to see elevation patterns in both air temperature and precipitation. Elevation patterns are unrefined in Fig. 2b, d, and e because the products with coarse spatial resolution and topography cannot resolve the complex temporal and spatial dynamics of mountain elevation ranges.

#### 2.3. Sentinel-1 snow depth retrievals

The data assimilation algorithm described in Section 2.5 integrates snow depth retrievals from Sentinel-1 backscatter observations (Lievens et al., 2019, 2022). The snow depth retrieval leverages the dependence of the radar C-band backscatter signal to the accumulation or ablation of snow and it uses a change detection method to derive snow depth values (Lievens et al., 2019). The snow depth algorithm takes advantage of the fact that snow is a dense medium of clustered, irregularly shaped ice crystals that contribute to volume scattering. Moreover, increased scattering can originate from snow layer interfaces and snow-ground interactions. A deeper snowpack generally results in stronger scattering, thus the strength of the scattering can be related to snow depths. The retrieval quality is best for dry snow with mean absolute error values of 17-18 cm according to Lievens et al. (2022). However, the dataset also contains retrievals of wet snow (marked with an associated flag). In this work, we include both dry and wet flagged observations, and increased the associated uncertainty to 30 cm. We only assimilate retrievals up to snow depth peak time. While this helps to remove springtime wet-flagged observations, assimilating retrievals before peak time also allows to better isolate the snow depth dynamics linked to snowfall orographic accumulation. The snow depth peak time is determined directly from the Sentinel-1 retrievals. Although the study region of this work has a greater frequency of available observations, we downsized the availability of Sentinel-1 observations to check whether the proposed methodology would also work in other areas (e.g. the Western United States Mountains or the High Mountains of Asia) where observations are not as frequently available (Lievens et al., 2019). For this

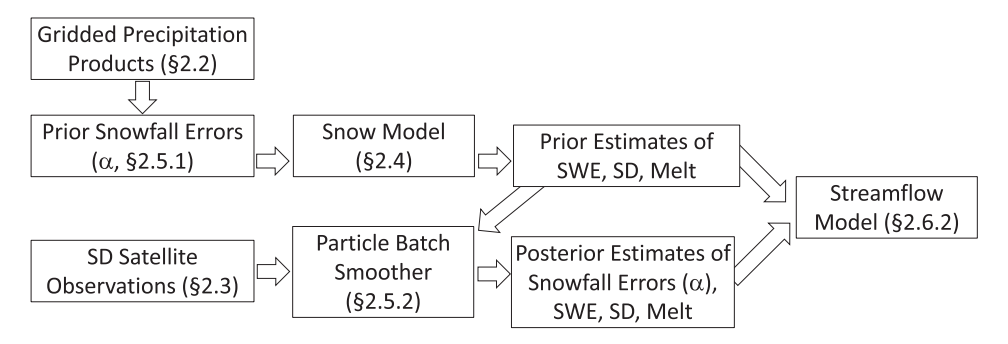


Fig. 1. Schematic representation of the methods used and associated Section (§) where each component is described.

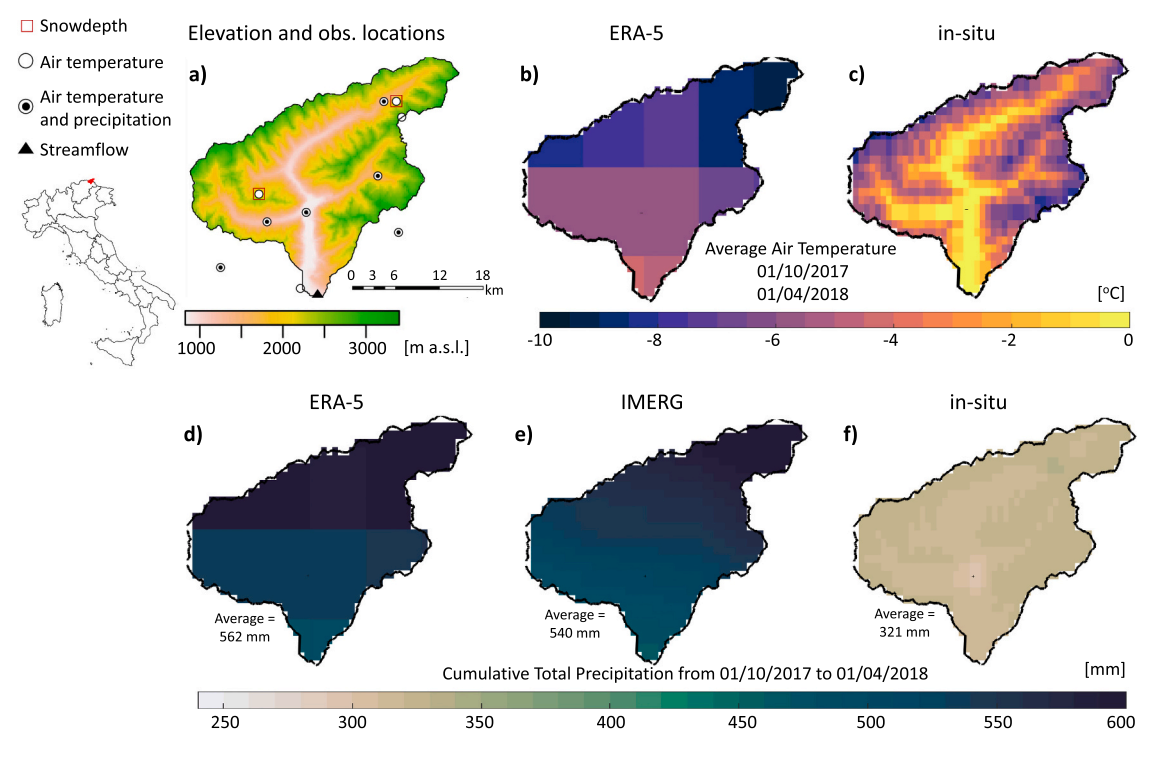


Fig. 2. a) European Digital Elevation Model (m above sea level, a.s.l.) for the domain of interest; b) ERA-5 and c) in-situ average 01 Oct. 2017 to 01 Apr. 2018 air temperature; d) ERA-5, e) IMERG, and f) in-situ cumulative total precipitation for the period 01 Oct. 2017 to 01 Apr. 2018, with spatial averages indicated in the insert text.

reason, the assimilation step only uses a subset of the available Sentinel-1 snow depth retrievals, as we sample them with a 15 days frequency. Data can be freely accessed via https://ees.kuleuven.be/project/c-snow.

#### 2.4. Snow model

The approach presented here is applicable to any physically based or empirical based (e.g., temperature index) snow models capable of estimating snow depth values. In this work we use a very simple model, the SNOW-17 snow accumulation and ablation model (Anderson, 1973). The primary variable of interest of this work is the characterization of snowfall uncertainty, which is expected to be approximately the same regardless of the level of complexity of the snow model. If anything, the results obtained using a simplistic model should be conservative and by simulating snow dynamics with a better model should just improve upon the results reported in the present analysis. SNOW-17 has also been used for years by the National Weather Service River Forecast System (Anderson, 1973). It solves a simplified snow energy balance that accounts for snowpack accumulation, heat exchange between the snow and air temperature, snow cover extent, heat storage and exchange, and water retention or transmission. The only two required dynamic inputs are total precipitation and 2 m height air temperature. Snow density is calculated using time-based algorithms that account for snow aging, mechanical compaction, and the impact of liquid water with adjustments for new snow deposition. We replaced the original snow density scheme with the iSnobal parameterization (Marks et al., 1999) which has been extensively adopted by the snow scientific community across a wide range of scales and mountain environments (Painter et al., 2016; Hedrick et al., 2018).

Normally, SNOW-17 must be calibrated to produce quality simulation results. This could be done by both using snow depth and SWE observations (which are scarce - if not absent - in many mountainous regions) and/or by embedding the snow model in rainfall-runoff models to calibrate against streamflow data (which are also scarce over mountainous regions). Calibration does not always guarantee optimal results

especially when the number and length of the time series of snow depth observations is limited. SNOW-17 is most sensitive to the following parameters. 1) SCF (hereafter  $\alpha$  (–)) is the multiplying factor which adjusts precipitation that is determined to be in the form of snow. The coefficient  $\alpha$  primarily accounts for gauge deficiencies but also implicitly includes the net effect of vapor transfer (sublimation and condensation, including from intercepted and blowing snow) and transfers across areal divides. 2) MFMAX is the maximum melt factor during non-rain periods (mm/°C/6 h), set at the summer solstice; while 3) MFMIN is the minimum melt factor during non-rain (mm/°C/6 h), set at the winter solstice. 4) UADJ, the average wind function during rain-on-snow periods (mm/ mb). UADJ is only a major parameter when there are frequent rain-onsnow events with relatively warm temperatures. The sensitivity of the UADJ parameter has been assessed in several studies (Houle et al., 2017; Franz et al., 2008; He et al., 2011) Results, although they are very site specific, showed that the UADJ minimally affected the model outputs. 5) PXTEMP, the temperature that separates rain from snow (°C). If the air temperature is less than or equal to PXTEMP, the precipitation is assumed to be in the form of snow. In this work, these most critical parameters are assumed uncertain. That is, rather than specifying a unique value for each of the model parameters, we use an ensemble of possible values (Table 1). For other less sensitive parameters, we assume that the calibration at the in-situ locations is representative of the entire test basin. These were calibrated by maximizing the Kling-Gupta Efficiency index (KGE; Gupta et al., 2009) between snow depth model simulations and snow depth observations at the two in-situ snow depth locations (Fig. 2a) for the snow season 2018-2019 using a particle swarm optimization approach (Eberhart and Kennedy, 1995, https ://www.mathworks.com/help/gads/particleswarm.html) swarm size of 100, and chose the parameters from the one site that lead to maximum KGE value. Appendix A includes more details about the calibration. Note that the calibration of the model has the only objective of reducing SNOW-17 model uncertainty to approximate realistic snow conditions, i.e., by generally relating in-situ precipitation to in-situ snow depth at two locations during 1 year.

**Table 1**Perturbation values to generate the ensemble of prior snow depth estimates. The table also lists types and magnitude Multiplicative (M), Additive (A), or Uniform (U) of the sampling distributions used for each of the perturbed variable. The magnitude (Magn.) of the perturbations is defined by the standard deviation ( $\sigma$ ), or the coefficient of variation (CV), or the minimum and maximum range (Range), for the additive, multiplicative, uniform perturbation types respectively.

	Type	Magn.	Range
Snowfall correction factor $(\alpha, [0, \infty])$	M	CV = 1	
Air temperature (°C)	A	$\sigma = 1$	
Maximum melt factor (MFMAX,[mm· $^{o}C^{-1}\cdot 6hr^{-1}$ ]	U		[1, 2]
Minimum melt factor (MFMIN,[mm $\cdot$ <sup>0</sup> $C^{-1}\cdot$ 6 $hr^{-1}$ ]	U		[0, 1]
Wind function rain-on-snow (UADJ, [mm⋅mb <sup>-1</sup> ])	U		[0.001, 0.1]
Rain- snow-fall temp. threshold (PXTEMP, [°C])	U		[0, 3]
Snow density parameters (C1-C5, CX, THRESD)	M	CV = 0.5	

## 2.5. Data assimilation approach

The assimilation approach uses an ensemble particle batch smoother, a generalization of the particle filter (Van Leeuwen, 2009). Being a Bayesian method, the conditional probability distribution of a variable of interest (in our case estimates of snowfall biases, quantified by  $\alpha$ ) can be determined from its likelihood function, and the probabilities of its prior distribution (before assimilation) along with those of the observations (in this case, Sentinel-1 snow depth retrievals). In an ensemble approach, these continuous probabilities are approximated by discrete distributions, with an ensemble of particles, each assigned a specific weight ( $w_i$ ). In contrast to a filter approach, a batch smoother (Margulis et al., 2015) allows the assimilation of multiple available observations in time at once (i.e., assimilation in batch and not sequential).

The assimilation approach follows two primary steps: 1) the generation of an ensemble of members (or particles, Section 2.5.1); and 2) update step where the Sentinel-1 snow depth retrievals are assimilated and the particle weights updated (Section 2.5.2). Each of these steps is done independently for the individual model grid cells (i.e., we assume no spatial correlation between model grid cells). We also repeat these steps for each of the water years one at the time, treating each of the years independently. In all these steps, the main assumption is that errors in modeled snow depth estimates are primarily caused by uncertainties in snowfall (i.e., snowfall biases,  $\alpha$ ) and the assimilation of observed Sentinel-1 snow depth retrievals allows us to estimate them.

## 2.5.1. Ensemble generation

The first step of the algorithm is to generate an ensemble of possible particles, meant to represent the probability density function of the model realizations prior to the assimilation. That is, we know that model estimates contain uncertainties that can be difficult to resolve and can potentially impact accurate estimates of snow depth. By generating an ensemble of possible model realizations, the data assimilation method avoids unrealistic confidence in the model estimates. To fully capture model uncertainties, the ensemble of realizations could be obtained from multi model simulations. In this work, we aim to represent model uncertainties by perturbing key parameters as described next. We use an ensemble size of 100 members (or particles,  $N_{ens} = 100$ ). Previous literature demonstrates that this number is large enough to stabilize performances of particle filter approaches (Han et al., 2021; Magnusson et al., 2017). The ensemble is generated via the perturbation of a series of model parameters and meteorological forcings as summarized in Table 1. Again, the underlying assumption is that most of the uncertainty comes from biases in snowfall (e.g., Raleigh et al., 2015). This is represented by perturbing the parameter  $\alpha$  (snowfall correction factor). Possible values of  $\alpha$  are sampled from a log-normal distribution with mean= 1.0 and coefficient of variation CV = 1.0 (Table 1). These values imply that perturbations are unbiased and, on average, correspond to 100 % of the magnitude of the nominal precipitation. We also perturbed other forcings and model parameters that are known to be uncertain and hard to calibrate (Section 2.4). These are listed in Table 1 and include perturbations of air temperature, and model parameters dictating melt factors (MFMAX and MFMIN), snow-density parameters (C1-C5, CX,

THRESD), wind function for rain-on-snow events (UADJ), and the temperature function to distinguish between rainfall and snowfall events (PXTEMP). Total precipitation is assumed to be all in the form of snowfall or rainfall if air temperature is less than  $-1^{\circ}$ C, or greater than  $3^{\circ}$ C, respectively. If the air temperature is between  $-1^{\circ}$ C and  $3^{\circ}$ C, only a fraction of the total precipitation is assumed to be snowfall based on the model parameter PXTEMP.

The generation of the ensemble also translate snowfall biases ( $\alpha$ ) (i. e., the assimilation control variable) into observation-like variables (i.e., snow depth observations). For this, we run SNOW-17  $N_{ens}$  times, each time using a different suite of inputs as obtained by the ensemble generation step (Section 2.5.1). The ensemble generation step generates (among others) an ensemble of  $N_{ens}$  precipitation biases ( $\alpha$ ), and snow depth particles. Prior to the update step (Section 2.5.2), each of these particles has the same probability of occurrence that corresponds weights equal to:

$$w_j^- = \frac{1}{N_{ens}}; \sum_{i=1}^{N_{ens}} w_j^- = 1 \tag{1}$$

## 2.5.2. Update step

The goal of the update step is to renew the weights of the ensemble particles (Eq. 1) by assimilating Sentinel-1 snow depth retrievals. This is done by calculating the observations likelihood function  $p_{Z|Y}(Z|Y)$ , where Z corresponds to an array containing all Sentinel-1 snow depth retrievals within the assimilation window (i.e., the entire water year) and Y is the assimilation control vector. In our case, Y contains the  $N_{ens}$  values of snowfall biases  $\alpha$ . The likelihood function corresponds to the specified probability distribution function for the observation errors,  $p_V \left(Z - M_j^-\right)$ , of size  $N_{obs}$  (i.e., number of retrievals in the assimilation window), where  $M_j^-$  is predicted snow depth from ensemble member j. The data assimilation scientific community often refers to  $\left(Z - M_j^-\right)$  as the "vector of innovations". The probability distribution function for the observation errors,  $p_V \left(Z - M_j^-\right)$  is typically represented by Gaussian processes where observation errors are assumed to have zero mean and a specified  $C_V$  error covariance:

$$p_{\nu}\left(Z - M_{j}^{-}\right) = \frac{1}{\sqrt{|C_{\nu}|}\sqrt{2\pi^{N_{obs}}}} e^{-\frac{1}{2}\left(\left[Z - M_{j}^{-}\right]^{T}|C_{\nu}|^{-1}\left[Z - M_{j}^{-}\right]\right)}$$
(2)

Assuming observations have negligible autocorrelations when compared to the specified single observation errors, we can treat  $G_{\nu}$  as a diagonal matrix with the diagonal values corresponding to the assumed observations error standard deviation (Section 2.3). The updated particle weights are calculated by:

$$w_{j}^{+} = \frac{C_{0}}{N_{ens}} p_{v} \left( Z - M_{j}^{-} \right) \tag{3}$$

where  $C_0$  is an integration constant and it is obtained from constraining the likelihood function to be a valid probability distribution ( $\sum_{j=1}^{N_{ons}} w_j^+ = 1$ ):

$$C_{0} = \frac{N_{ens}}{\sum_{j=1}^{N_{ens}} p_{v} \left( Z - M_{j}^{-} \right)}$$
(4)

This process assigns higher weights to the "more likely" particles because their snow depth prediction  $(M_i^-)$  is closer to the observed values (*Z*). Conversely, the process reduces the weights of those particles whose observation error is higher (i.e., snow depth estimates and observations are farther apart). A typical issue associated with sequential particle filters is the collapse of the ensemble, occurring when too much weight is assigned to only a few particles (those similar to the observations). In such case, resampling techniques are used to guarantee a adequate ensemble spread. In this work, resampling was not done since we assimilate all observations occurring in one water year at once (in a batch rather than sequential format). The updated weights (Eq. (3)) provide a discrete estimate of the posterior probability distribution which can be used to determine posterior statistics of the  $\alpha$  distribution, and consequently our updated snowfall variable. The update weights can also be used to calculate statistics and ensemble percentiles for other variables of interest such as snow water equivalent, snow melt, and snow depth. In this article we present results for the percentiles 25 %, 50 %, and 75 % (i.e., the interquartile range), as well as mean and standard deviation statistics.

## 2.6. Experimental setup and evaluation criteria

We tested the methods for water years 2016, 2017, 2018, and 2019. For the example of year 2016, the water year is defined as the period that goes from 01 October 2015 to 30 September 2016.

We developed three experiments each using a different combination of atmospheric forcings (Section 2.2): 1) "in-situ", where air temperature and precipitation are both from the in-situ observations; 2) "ERA-5", where both air temperature and precipitation are derived from the gridded ERA-5 atmospheric reanalysis product; 3) "IMERG", where air temperature is taken from in-situ observations and precipitation from IMERG. The "in-situ" case could be considered the best possible scenario since both precipitation and air temperature are locally observed, thus considered more representative of the basin dynamics. The "ERA-5" configuration could be seen as representative of those scenarios that would be adopted in data-scarce regions where in-situ observations might be lacking. Finally, the "IMERG" scenario can be seen as a more sophisticated case with respect to the previous configuration because of the elevation aware air-temperature inputs (in-situ air temperature) allow for orographic partitioning of rainfall vs. snowfall; further, the satellite-derived precipitation (IMERG) allows for a precipitation product that is directly observed rather than modeled. This last experiment setup could be seen as representative of applications where gridded precipitation products are used along with some downscaling techniques to represent local-scale orographic dynamics (e.g., Girotto et al., 2014; Wang et al., 2019; Xue et al., 2021). The methods are evaluated using independent variables of snow cover area (Section 2.6.1) and streamflow (Section 2.6.2). We only assimilate one Sentinel-1 retrieval every 15 days as we want to ensure the robustness of the method to be applied in regions where the Sentinel-1 retrievals are not as abundant as they are in our test domain (Section 2.3).

## 2.6.1. Snow cover area

A basin-wide 8-day averaged observation of the fractional snow cover area estimates is calculated from the MODIS MOD10A1 (Hall et al., 2002) data collection. We compare it to both the prior (results from the ensemble generation, Section 2.5.1) and posterior (after the assimilation of snow depth) fractional snow covered estimates to evaluate the performances of the proposed method. The snow model does not directly include a snow depletion curve to estimate fractional snow cover area; thus, we estimate it in a binary way. That is, for each basin grid cell we assign a snow cover fraction of 0 % or 100 % depending on

whether the prior (or posterior) SWE is above or below a specific threshold of 40 mm (De Lannoy et al., 2010). From the basin-wide average of these binary values of snow cover areas, for each day, we calculate the percentage of the basin that is covered in snow. These values are further smoothed and aggregated to an 8-days average. Using them, we calculate Pearson correlation coefficients between the observed (MODIS) and modeled (prior and posterior) fractional snow cover area.

## 2.6.2. Streamflow

Once we determine the spatially varying updated or posterior ensemble mean SWE, and most importantly snow-melt (or melt-driven discharge), we use their values to initialize the lumped hydrological model HYMOD (Moore, 1985), in order to obtain streamflow estimates at the outlet of the basin. Hymod is a simplified lumped hydrological model which is based on the ideas presented in Moore (1985) of probability-distributed infiltration capacity and storage capacity and implemented by Boyle (2001) and has been widely applied across a variety of climates, spatial and temporal scales (Wagener et al., 2001; Formetta et al., 2011; Abera et al., 2017; Vrugt et al., 2003). The model receives rainfall, snow melt, and potential evapotranspiration time series as input and provides the discharges at the outlet of the basin as main output. We subset the streamflow time-series in two halves, the first half of the simulation period has been used for the calibration and the second half for validation.

For the validation subset we evaluate performances of the different assimilation experiments using the KGE coefficient. On top of this, we compared prior and posterior streamflow simulations in terms of flow duration curves to look at the entire streamflow distribution.

#### 3. Results

## 3.1. Precipitation biases

The precipitation correction factors estimated via snow depth data assimilation are shown in Fig. 3. The "In-situ" derived snowfall tends to underestimate the basin-wide amount of snowfall in the basin as the average value of  $\alpha$  for in-situ forcings is greater than one (Fig. 3a). Similarly, with the exception of water year 2017, the "IMERG" scenario also underestimates the basin-wide snowfall (Fig. 3c) as the basin-averaged  $\alpha$  is greater than one. These results suggest that for both "in-situ" and the "IMERG" scenarios, snowfall needs multipliers ( $\alpha$ ) greater than one in order to obtain snow depth estimates comparable with those retrieved by Sentinel-1. Conversely, "ERA-5" snowfall tends to overestimate the average amount of snowfall in the basin (Fig. 3b) with average  $\alpha$  values less than one.

Regardless of the actual basin-wide numbers in these figures, the spatial distribution of  $\alpha$  (Fig. 3) indicates a strong elevation dependency on the distribution of the snowfall errors. Across the three experiments (Fig. 3), smaller  $\alpha$  values, typically less than one, correspond to lower elevations (i.e., reducing snowfall amounts); and the larger  $\alpha$  values, generally greater than one, correspond to higher elevations (i.e., increasing snowfall amounts). In other words, the assimilation scheme adjusts the prescribed snowfall by reducing snowfall at the lower elevations, where model snow depth is likely overestimated with respect to the Sentinel-1 retrievals, and by increasing it at the higher elevations where modeled snow depth is underestimated. The  $\alpha$  spatial patterns highlight the hidden positive feedback of the proposed assimilation scheme: it effectively downscales the coarser spatial resolution of the gridded precipitation estimates. That is, the assimilation of the 1 km resolution snow depth retrievals provides a way to inform the large-scale precipitation product (i.e., ERA-5 or IMERG) on how to be adjusted at a local scale in order to provide consistent finer resolution snow depth estimates. Despite the small sample of years, the 4-year spatial mean and standard deviation (non-shown here) suggest that the snowfall multipliers  $\alpha$ , tend to be interannually consistent. The in-situ experiment

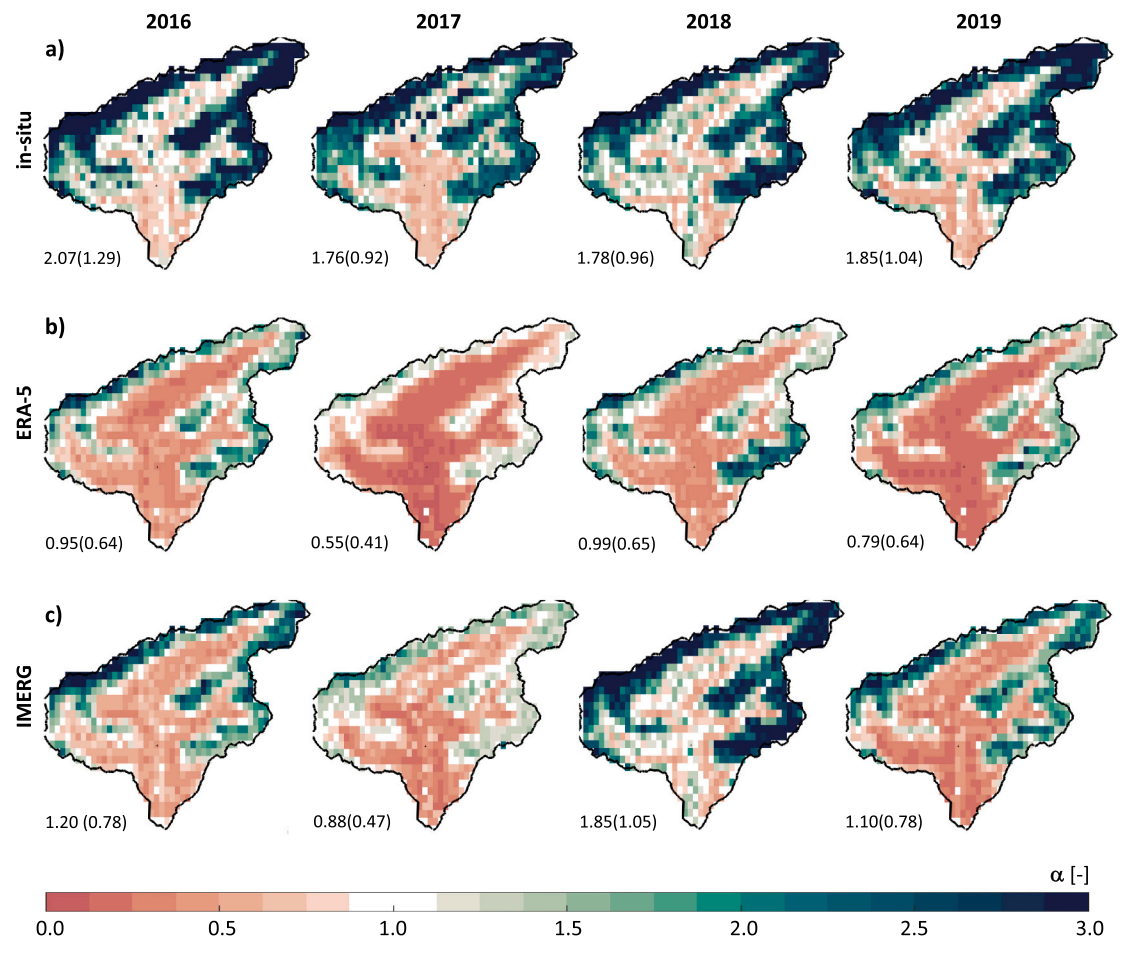


**Fig. 3.** Snowfall correction factor estimates (α) for experiments with a) in-situ; b) ERA-5; c) IMERG precipitation products. (Left to right) maps indicate water years 2016; 2017; 2018; and 2019. The numbers reported in each map correspond to the spatial average (standard deviation) values of the snowfall biases, α.

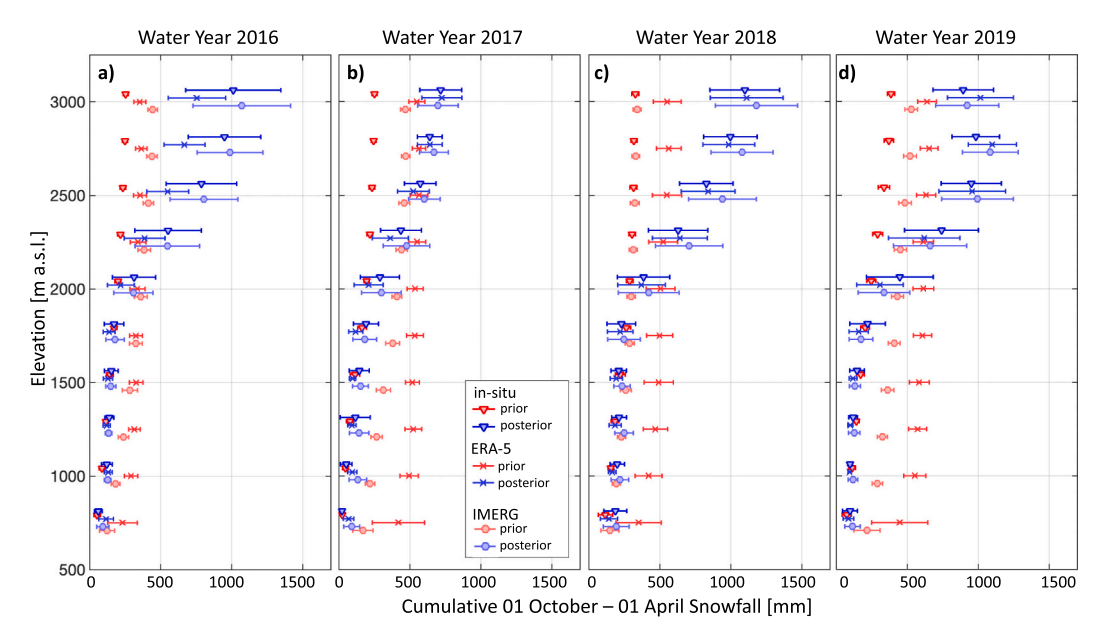


Fig. 4. Cumulative snowfall for the period 01 October to 01 April of each water year binned by elevation bands of 250 m. For each of the 250 m elevation bands, three marker types represent the three different forcings (in-situ, ERA-5, and IMERG, Section 2.6) for both prior (model-only, red markers) and posterior (data assimilation, blue markers) snowfall estimates. Each error bar shows the mean and standard deviation of the cumulative snowfall of that specific elevation band.

leads to the most uniform interannual variability (i.e., consistently less variability in the snowfall errors) possibly due to combined prior (before assimilation) spatial distribution of both in-situ precipitation and air temperature observations used for this experiment as these are likely more accurate than the gridded products.

## 3.2. Orographic snowfall patterns

The precipitation biases shown in Fig. 3 exhibit spatial features that help define spatial distribution of the resulting snowfall across the domain. Here, we discuss the elevation patterns of snowfall patterns, that is the spatial variability of snowfall as a function of elevation, as reported by Fig. 4.

For the prior snowfall elevation patterns, when compared to the "ERA-5" and "IMERG" scenarios, the "in-situ" leads to the smallest cumulative amounts of snowfall across all elevations and years (downward facing red triangle markers, Fig. 4). This result is consistent with the differences in precipitation magnitude seen for the sample year shown in Fig. 2d-f. Across all forcing datasets, the prior snowfall estimates (red markers) show little changes in the accumulated snowfall as a function of elevation. That is, snowfall elevation gradients are small and nearly zero indicating that snowfall accumulation does not increase with elevation. Special cases are the "in-situ" and "IMERG" prior estimates presenting a small elevation gradient in their elevation distribution (i.e., triangle and circle red markers move toward higher accumulation as the elevation increases, Fig. 4) caused by their orography dependent in-situ air temperature (Fig. 2c). This is not the case for the coarse-scale reanalysis product ("ERA-5") where the elevation patterns are nearly absent in the prior simulations (red crosses) because of the unrefined elevation dependency in the ERA-5 forcings (Fig. 2b, d).

Across all years and experiment scenarios, the posterior estimates (blue markers) lead to a more noticeable elevation gradient where

cumulative snowfall values increase as a function of elevation. In general, across the four years, the location of the mean accumulated snowfall distribution and the spatial variability (standard deviation represented by the error bar), aligns well across the three forcings scenarios (best case is Fig. 4b and d). An exception to this general result is seen in the posterior cumulative snowfall around 2000–3000 m a.s.l. for water year 2016 when "ERA-5" experiment lead to smaller amount with respect to the "in-situ" and "IMERG" scenarios (blue triangles and circles vs. blue crosses, Fig. 4a). The elevation dependent in-situ air temperature, used by the first two experiments, boosts the snowfall orographic gradient for this year.

Regardless of the prior (model-only) precipitation product, the assimilation of Sentinel-1 snow depth leads to similar elevation dependent cumulative snowfall patterns where the snowfall accumulation gradient is modest for elevations below 1500 m a.s.l., it strongly increases from the elevations 1500 m a.s.l. until 2500 m a.s.l., and it is modest for elevations above 2500 m a.s.l. In fact, for elevation above 2500 m a.s.l., the accumulated snowfall does not increase as strongly with elevation (best case is illustrated by Fig. 4d), possibly due to atmospheric moisture saturation effects. The obtained posterior elevation patterns suggest that the spatial (elevation) distribution of snowfall is in general consistent and robust across the chosen prior set of forcings.

## 3.3. Snow depth and snow cover area

Evaluating the assimilation performance using the assimilated snow depth values does not constitute an independent validation yet it provides a means to internally check assimilation performances. For the example location shown in Fig. 5, when the model uses "in-situ" forcings, it delivers snow depth values that underestimate the observed ones (i.e., prior estimates are lower than the observed Sentinel-1 retrievals Fig. 5a). Similarly, the "IMERG" scenario tends to underestimate snow

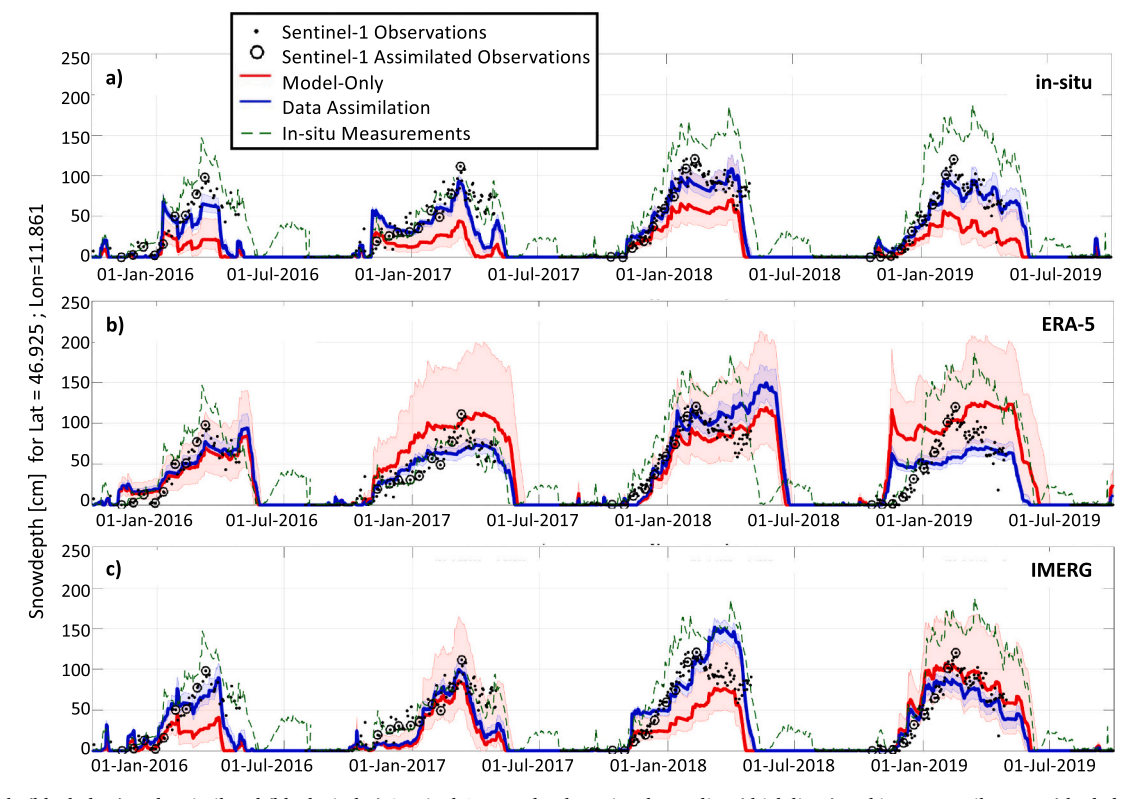


Fig. 5. Available (black dots) and assimilated (black circles) Sentinel-1 snow depth retrievals, median (thick lines) and inter-quantile range (shaded area) of prior (or model-only, red) and posterior (or assimilation, blue) snow depth estimates for a sample location at 2155 m a.s.l. elevation lat = 46.92° lon = 11.86° and for the case when the model runs with a) in-situ air temperature and in-situ precipitation; b) ERA-5 air temperature and ERA-5 precipitation; and c) in-situ air temperature and IMERG precipitation. For reference, the in-situ (point-scale) snow depth observations are also shown (dashed green).

depth values for all years, with the exception of water year 2019 Fig. 5c). In contrast, "ERA-5" scenario leads to values of prior peak snow depth that are consistent with those observed by Sentinel-1 (Fig. 5b).

When looking at the ensemble spread (i.e., uncertainty) of the prior estimates, for the "ERA-5", and "IMERG" experiments, most of the Sentinel-1 retrievals are included within this uncertainty range (Fig. 5b–c); whereas for the "in-situ" case, retrievals are located at the edges of the prior ensemble interquartile range (Fig. 5a). For an optimal assimilation condition, we would want the retrievals to be assimilated to all be included within the ensemble of possible model realizations (i.e., the red envelope in Fig. 5).

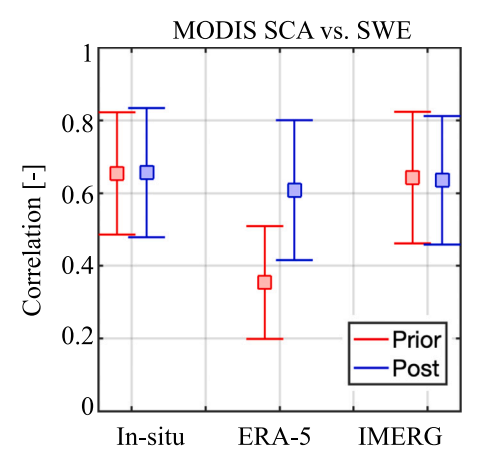
Regardless of the prior simulations of snow depth, the proposed assimilation scheme leads to posterior estimates of snow depth that correspond better with those observed by Sentinel-1 (blue estimates in Fig. 5). The posterior estimates also reduced the ensemble spread for each of the four forcing scenarios. This means that, while the posterior snow depth estimates are expected to be more robust and less uncertain, their drastically reduced uncertainty is likely too optimistic. The overly optimistic approximation of the posterior ensemble spread is typically seen as a limitation of particle filters. The limitation improves, but it is not entirely solved by smoothers assimilation approaches (Margulis et al., 2015).

Fig. 6 shows the monthly prior and posterior snow depth estimates for February 2018 for all three forcing scenarios, alongside Sentinel-1 estimates. Sentinel-1 snow depth (Fig. 6a) indicates a distinct elevation pattern, with naturally deeper snow depths located at higher elevations (compare Figs. 6a to 2a). Elevation patterns are visible when estimating snow depth using "in-situ" and "IMERG" (Fig. 2b and d). These are likely caused by the spatial distribution of air temperature (Fig. 2) that partitions precipitation into snowfall and rainfall amounts. Despite having an elevation gradient, when compared to Sentinel-1 retrievals, the "in-situ" and "IMERG" prior experiment leads to 58.6 cm and 59.9 cm respectively of basin-wide snow depth and thus underestimates Sentinel-1 (Fig. 2b, d). In the ERA-5 case, the prior distribution of snow depth is unrealistically blocked due to the coarse resolution of the product. Despite having unrealistic spatial patterns, the magnitude of the basin-wide snow depth values produced by "ERA-5" is 107.3 cm and more comparable to those in Sentinel-1. In all cases ("insitu", "ERA-5", and "IMERG") snow depth values underestimate the basin-wide value in Sentinel-1 (Fig. 6a).

The assimilation results from all three experiments lead to basin-

wide values that are closer (within 6 cm differences) to those reported in Sentinel-1 (Fig. 6e–g). Regardless of the spatial patterns of the prior distribution, the assimilation brings more realistic snow depth elevation gradients that assign snow to the higher elevations. This result is consistent with the patterns obtained by snowfall and precipitation error coefficients as described in Sections 3.1 and 3.2.

An independent evaluation using the MODIS fractional snow cover dataset is shown in Fig. 7. Furthermore, the evaluation of the spatial distribution of snow cover (Fig. 7) can be seen as a tool to assess the accuracy of snow depth spatial distribution. The spatial correlation skill values against MODIS fractional snow cover is best for the prior experiment that uses in-situ and IMERG precipitation, with a temporal average values of 0.65 and 0.66, respectively. The correlation values are weaker for the ERA-5 prior simulations with associated skill value of 0.35. Higher spatial correlations values might be expected for the in-situ and IMERG experiments considering the given a-priori realistic spatial distribution of the air temperature (Fig. 2c) that contributes to a realistic spatial distribution of snow depth in the basin, albeit underestimated in



**Fig. 7.** Snow Cover Area (SCA) correlations between MODIS and the fractional snow cover estimated from the prior and posterior snow water equivalent values. Each error bar represent the 2016–2019 average and one standard deviation of the correlations computed from each of the 8-days snow cover area composite (Section 2.6.1).

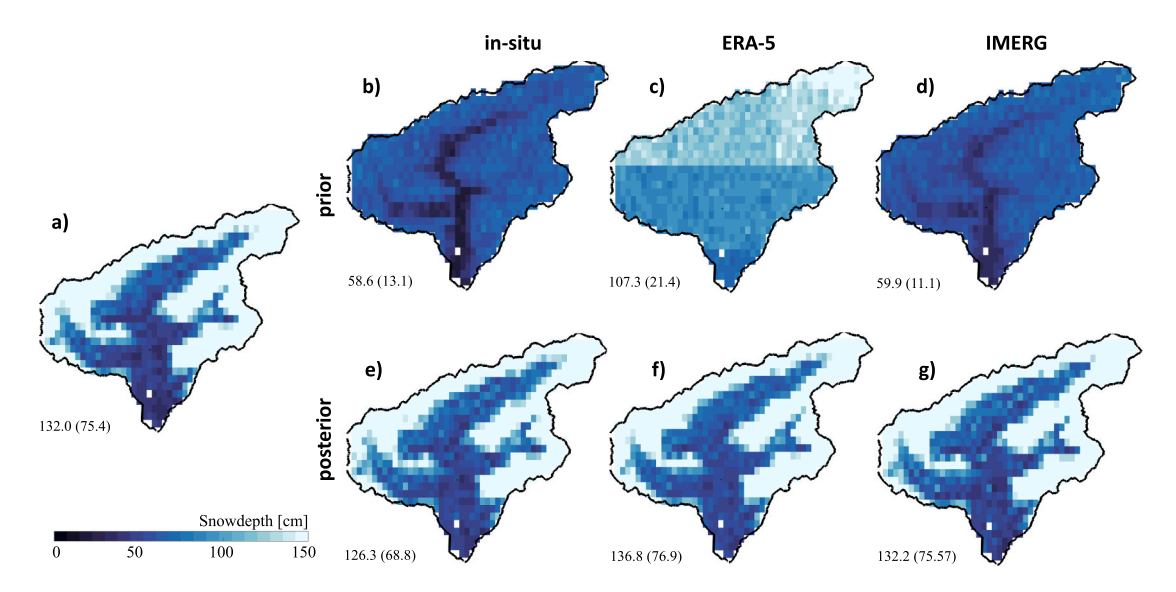


Fig. 6. Water year 2018 monthly averaged February snow depth estimates a) observed from Sentinel-1; and estimated from Snow-17 (prior) using b) in-situ air temperature and precipitation ("in-situ"); c) ERA-5 air temperature and precipitation ("ERA-5"); d) in-situ air temperature and IMERG precipitation ("IMERG"). The bottom row shows the corresponding estimated monthly averaged February snow depth values that result from the assimilation of Sentinel-1 retrievals when using e) "in-situ"; f) "ERA-5"; and g) "IMERG" scenarios.

magnitude (Fig. 6b, d). For the posterior cases, the correlation values are consistently centered at around 0.61–0.66 for all three experiments. This conveys that regardless of the input forcing, the assimilation of snow depth retrievals leads to MODIS snow cover area consistent spatial patterns. This is particularly noticeable for the ERA-5 experiment, for which the spatial patterns improve the distribution of snow on the ground (i.e., posterior correlation values are higher than the respective prior ones). No improvement is obtained when using in-situ or IMERG forcings. Again, this can be caused by the already modest spatial patterns brought by the elevation dependent in-situ air temperature (Fig. 2c).

#### 3.4. Streamflow

The snow depth and orographic precipitation improvements as indicated in the previous result sections are tightly linked to streamflow. Furthermore, besides biases in snowfall estimates, the values of  $\alpha$  could also be influenced by biases in air temperature. That is, even if the total precipitation is unbiased, warm biases in air temperature can lead to more rainfall and less snowfall. The assessment of streamflow can be seen as a more holistic way to verify whether the adjustments are due to biases in air temperature or actual precipitation.

Observations of streamflow suggest that the river flow is dominated by snowmelt as the flow peaks during snow melt season and, depending on the year, reaches values of  $75-85\ m^3/s$  (Fig. 8). Both prior and posterior assimilation estimates predict the timing of the observed

seasonality correctly, however the magnitude of both peak and low flows varies and are different from the observed ones. In general the posterior streamflow peaks tend to represent observations better than the prior estimates. This is especially visible for the in-situ case (Fig. 8a). This means that the timing of snow melt during the spring and summer months is improved by the assimilation of snow depth values. Once again, this suggests that the assimilation of Sentinel-1 retrievals leads to better spatial patterns in the snow distribution across the entire basin (as discussed in Section 3.3). That is, areas with lower elevations are characterized by shallower snowpack; whereas the areas with deeper snowpacks are located at higher elevations. In general, as summer comes, the higher elevation releases water via snowmelt more slowly than the prior case (i.e., slower melt rate due to colder temperature, and longer travel time from higher elevation to the stream bed), which better matches the timing of the streamflow observations.

To better understand if there are benefits to the assimilation, Fig. 9 reports the flow duration curves (i.e., a cumulative frequency curve that shows the percent of time specified discharges were equaled or exceeded during a given period) where the flow distribution obtained from all 4 years from the posterior simulation (blue lines) agree better with the observations (black lines) with respect to the prior estimates (red lines). This result suggests that the assimilation of snow depth observations improves streamflow estimates especially for high flows which are occurring during summer months. A confirmation of this result is reported in Table 2 where the KGE of the streamflow values (obtained during the validation period 2018–2019) indicate that the assimilation

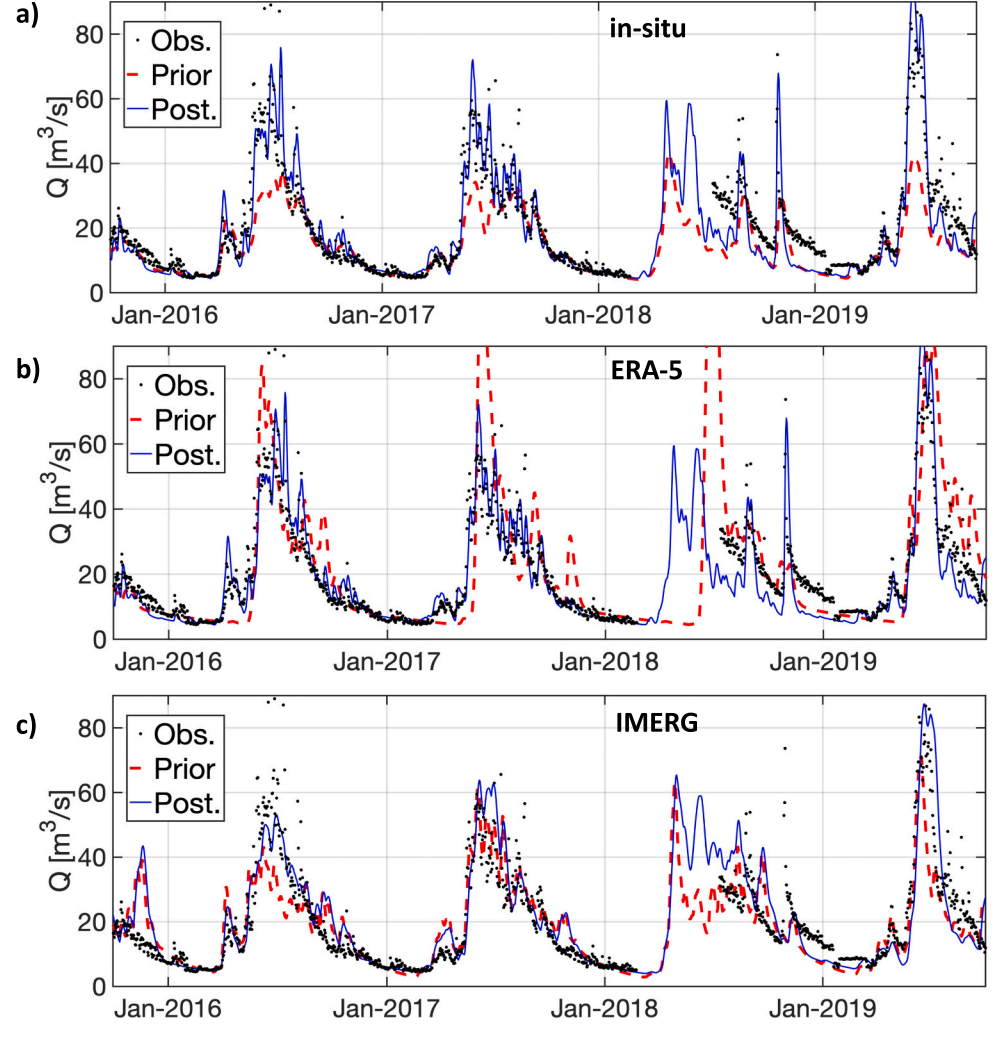


**Fig. 8.** Observed and estimated streamflow  $(m^3/s)$  at the basin outlet.

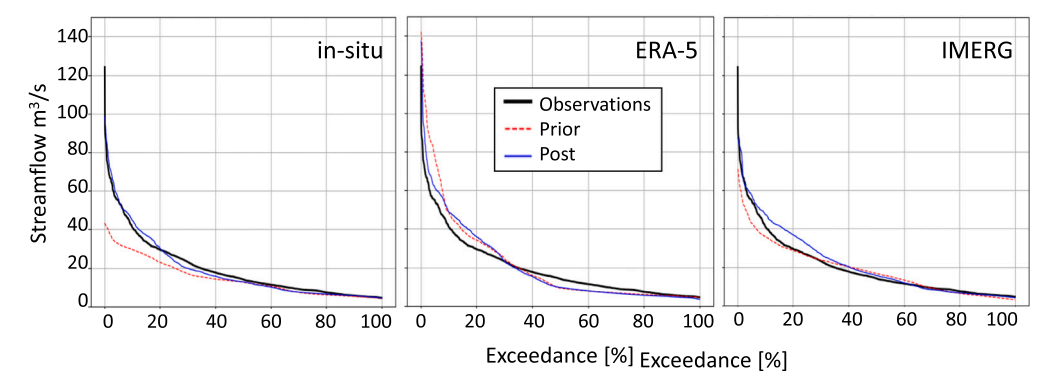


Fig. 9. Flow duration curves using daily streamflow discharge  $(m^3/s)$ .

**Table 2**Kling-Gupta Efficiency index calculated on using daily streamflow values (KGE). Only validation statistics are reported.

	In-situ		ERA-5		IMERG	
	Prior	Post	Prior	Post	Prior	Post
KGE	0.38	0.75	0.65	0.67	0.68	0.75

of snow depth retrievals results in improved streamflow estimates (of about 40 % on average). Fig. 9 also shows that the performances of the priors are not the same, with the in-situ prior having a lower performance compared to the ERA-5 and IMERG prior. This is a common issue when conceptual hydrological models are recalibrated for each prior type, which can be attributed to the strong interactions between the nonlinear model structure and the analyzed input data (e.g., Qi et al., 2016; Mei et al., 2016; Camici et al., 2018).

## 4. Discussion

In this work we test the hypothesis that snowfall orographic patterns can be retrieved using information about the snow depth that accumulates on the ground. This principle was introduced in Avanzi et al. (2020), in which in-situ snow depth observations were used. Here we extend this assumption to demonstrate that we can derive orographic precipitation patterns over seasonal snow dominated mountainous regions via the assimilation of readily available snow depth retrievals from Sentinel-1 (in agreement with the operational overpasses of the satellite). We argue that our proposed method, despite being assessed only over a test basin in the Alps (the Aurino), provides a framework for correcting snowfall across any mountain area. The chosen domain is characterized by orographic complexity, and seasonal accumulation and melt dynamics. The Italian Alps can be assumed representative of other high elevation watersheds around the world that are similarly defined by orographic complexity and seasonal snowpack dynamics. Being in the Mediterranean climate, Aurino also features a high interannual climate variability (Cid et al., 2017). Because of this, it can be considered a good test domain to validate the approach proposed here since predicting Aurinos's snowfall spatiotemporal variability can be extremely challenging. Being in the Mediterranean climate, Aurino also features a high interannual climate variability (Cid et al., 2017) as it sits on the edge of the alpine divide between Southern and Northern Alps (Avanzi et al., 2023; Matiu et al., 2020; Prein and Gobiet, 2017), as well as receiving precipitation from both south and north storm fronts (Bertoldi et al., 2023).

The generality of the approach is further tested as we use three different precipitation products, each of which is sub-optimal across world-wide mountainous regions (Wrzesien et al., 2019). The assimilation of the Sentinel-1 snow depth retrievals provides a way to inform these uncertain large-scale precipitation products. We found a strong

elevation dependency on the distribution of the snowfall errors. These results are consistent with previous studies aimed at characterizing how winter precipitation increases as a function of elevation (e.g., Lundquist et al. (2010)). Consistent with Kang et al. (2021) we also found that the improved orographic precipitation patterns, and therefore robust spatiotemporal distribution of snow accumulation, leads to better estimates of the spring and summer streamflow, the key variable of interest for many of the downstream water resources managers.

## 4.1. Assumptions and limitations

There are some important limitations that should be discussed, as summarized next.

- 1. The key assumption that snowfall orographic patterns can be retrieved using snow depth ground accumulation can fail over regions with significant snow redistribution due to processes such as wind and/ or avalanches, or because of snow structure and density uncertainties (changing the relationship between precipitation water equivalent and snow depth). While we included uncertainties on key snow density parameters, a more accurate uncertainty analysis might be needed for other snow structure model parameters. For the specific domain and spatial scales (1 km), we assume snow redistribution processes are negligible relative to snowfall accumulation, but these processes could be significant for other regions or if targeting finer spatial resolutions (e. g., Clark et al., 2011; Mott et al., 2018). A solution to these limitations could be the application of the proposed assimilation scheme within a more sophisticated snow model and higher spatial resolutions (i.e., one capable of modeling wind redistribution and avalanche) so that snow redistribution processes are taken into consideration.
- 2. Sentinel 1A and 1B missions are characterized altogether by a revisit time of about 6 days in Europe (12 days now with the failure of the 1B satellite). While this revisit time is likely sufficient for snow depth data assimilation for a full snow season (e.g., Margulis et al., 2019), it can impact the correction of specific snowfall events. That is, a stronger link between precipitation and snow depth patterns might be achieved with frequent retrievals (e.g., Brandt et al., 2020), capturing the majority of precipitation snow accumulation events. Precipitation dynamics are often characterized by large variability in space and time and its signal is inherently erratic. In our experiments we assimilate one Sentinel-1 retrieval per month, and relying on more retrievals could help to improve upon the precipitation corrections shown here. Furthermore, by assimilating all satellite derived snow depth retrievals for the yearlong accumulation window, we assume that on average precipitation biases are consistent across snowfall storms, yet proportional to the amount of snowfall. Using a more frequent assimilation window (e.g., particle filter) could overcome this limitation.
- 3. Uncertainties in Sentinel-1 snow depth retrievals can be large in the presence of wet snow (Lievens et al., 2022) because of absorption of radar backscatter signal, or in areas with shallow and intermittent snow cover, resulting in poor snow depth estimates. To overcome these issues,

we limit the assimilation of the retrievals to only the accumulation season (i.e., prior to peak). More generally, future work could use the product provided "wet-flag" (Lievens et al., 2022) to exclude from the assimilation highly uncertain snow depth. A significant help in this respect could also be derived from the new method to map wet snow from Sentinel 1 data (Karbou et al., 2021).

4. Lastly, in this article we present results from a 4-years set of experiments, in agreement with the availability of assimilated and in-situ data. While the length of this period is enough to test the robustness of the proposed methodology, a longer data set should be employed to extract long-term spatial patterns of snowfall precipitation (Jimeno-Sáez et al., 2020).

### 5. Summary and conclusion

A skillful characterization of mountain hydrology is a challenging task particularly because of the lack of precise and accurate snowfall measurements across the complex terrain that characterize mountain ranges. This work characterizes snowfall orographic patterns by first identifying biases in commonly used snowfall products and then using observations to correct for the errors. We test the hypothesis that the assimilation of Sentinel-1 snow depth retrievals can identify and resolve orographic snowfall patterns in mountain catchments.

The analysis of the spatial characteristics of the snowfall elevation patterns suggests that the proposed assimilation scheme drives more accurate spatial patterns in the snowfall distribution across the entire basin. The retrieved snowfall orographic patterns lead to an overall improvement of mountain hydrologic variables such as snow depth, snow cover area, and streamflow. For streamflow, the largest improvements are reported during spring and summer months when peak flow observations agree better with the posterior cases rather than the prior ones. These results are primarily a consequence of the fact that assimilation of Sentinel-1 assigns less snowfall to lower-elevation regions of the basin whereas higher rates are assigned to the higher elevation. As summer comes, the higher elevation releases water via snow-melt more slowly than the prior case, which better matches observations.

While the prior snowfall cumulative elevation pattern has a small gradient across elevation bands, these patterns are consistent across elevations and precipitation products after the assimilation of snow depth retrievals. In other words, the assimilation of Sentinel-1

effectively downscales coarser-resolution precipitation products.

To conclude, this work provides the framework for correcting snowfall orographic patterns across other seasonally-snow dominated mountain area of the world, especially where in-situ data are scarce.

## CRediT authorship contribution statement

MG, CM: Conceptualization and Methodology; MG, GF, CM, MC, HL, SM: Data curation; MG: Formal analysis, and Writing of original draft; All authors contributed to review & editing.

#### Declaration of competing interest

The authors declare that they have no known competing financial interests or personal relationships that could have appeared to influence the work reported in this paper.

## Data availability

Data will be made available on request.

## Acknowledgements

This study was supported by NASA HiMAT team program (grant number 80NSSC20K1301); U.S. Department of Energy Computational Science Graduate Fellowship (award number DE-SC0022158); ESA projects 4D MED Hydrology (contract number ESA 4000136272/21/I-5 EF); DTE Hydrology Evolution (contract number ESA 4 4000136272/ 21/I-EF - CCN N. 1); and the NASA Terrestrial Hydrology Program (grant number 80NSSC22K0685). Sentinel-1A/B data are from the ESA and Copernicus Sentinel Satellites project and were processed using the ESA Sentinel Application Platform (SNAP). The Sentinel-1 snow depth retrievals have been supported by the BELSPO C-SNOW project (contract SR/01/375), with resources and services provided by the VSC (Flemish Supercomputer Center), funded by the Research Foundation – Flanders (FWO), the Flemish Government and KU Leuven C1 (C14/21/ 057). The authors declare no conflict of interest. The authors are grateful to the anonymous reviewers, whose comments improved the quality of this manuscript.

## Appendix A. Snow-17 calibration

The calibration exercise is accrued out using water year 2019 (i.e., from October 2018 through September 2019) to Kling-Gupta Efficiency index (KGE) equal to 0.869 and 0.9697 for the two in-situ snow depth locations (Fig. 2a) and using in-situ forcings (Section 2.2). Parameters obtained from the calibration with the highest values KGE are adopted for some of Snow-17 model parameters as described in Section 2.4. The list of calibrated model parameters for the two locations is listed in Table A.3. For reference the snowfall error coefficient  $\alpha$  obtained from the assimilation approach described in Section 2.5 are for site 1 and site 2 the corresponding 1 km grid cells are reported in Table A.4. Please note that for the most model sensitive parameters, these are assumed uncertain according to Table 1.

Table A.3 Parameter values obtained in the calibration of SNOW-17 model for the two in-situ locations (Fig. 2a.)

	Site ID (lat;lon)		
	Site 1 (46.92;11.86)	Site 2 (47.04;12.12)	
MBASE	1	0.8	
MFMAX	1.63	0.8	
MFMIN	0	0	
NMF	0.15	0.15	
PLWHC	0.04	0.04	
PXTEMP	1	1	
PXTEMP1	-1	-1	
PXTEMP2	3	3	
RSV	1	1	
		(continued on next page)	

(continued on next page)

#### Table A.3 (continued)

	Site ID (lat;lon)			
	Site 1 (46.92;11.86)	Site 2 (47.04;12.12)		
SCF (in this article, $\alpha$ )	1.70	3.13		
TIPM	0.1	0.1		
UADJ	0.001	0.012		

Table A.4
Snowfall biases (α) obtained from the assimilation approach described in Section 2.5 for the in-situ sites corresponding 1 km grid cells.

	Site 1				Site 2				
	2016	2017	2018	2019	2016	2017	2018	2019	
In-situ	1.44	1.40	1.07	1.30	1.12	1.68	0.88	1.55	
ERA-5	0.71	0.40	0.86	0.38	0.33	0.24	0.32	0.29	
IMERG	1.14	0.78	1.49	0.61	0.49	0.58	0.77	0.53	

#### References

- Abera, W., Formetta, G., Borga, M., Rigon, R., 2017. Estimating the water budget components and their variability in a pre-alpine basin with jgrass-newage. Adv. Water Resour. 104. 37–54.
- Anderson, E.A., 1973. National Weather Service River Forecast System: Snow Accumulation and Ablation Model, Vol. 17. US Department of Commerce, National Oceanic and Atmospheric Administration ....
- Avanzi, F., Ercolani, G., Gabellani, S., Cremonese, E., Pogliotti, P., Filippa, G., Morra di Cella, U., Ratto, S., Stevenin, H., Cauduro, M., et al., 2020. Learning about precipitation orographic enhancement from snow-course data improves waterbalance modeling. Hydrol. Earth Syst. Sci. Discuss. 2020, 1–37.
- Avanzi, F., Gabellani, S., Delogu, F., Silvestro, F., Pignone, F., Bruno, G., Pulvirenti, L., Squicciarino, G., Fiori, E., Rossi, L., et al., 2023. It-snow: a snow reanalysis for Italy blending modeling, in situ data, and satellite observations (2010–2021). Earth Syst. Sci. Data 15 (2), 639–660.
- Bandhauer, M., Isotta, F., Lakatos, M., Lussana, C., Båserud, L., Izsák, B., Szentes, O.,
  Tveito, O.E., Frei, C., 2022. Evaluation of daily precipitation analyses in e-obs (v19.
  0e) and era5 by comparison to regional high-resolution datasets in european regions.
  Int. J. Climatol. 42 (2), 727–747.
- Beck, H.E., Wood, E.F., Pan, M., Fisher, C.K., Miralles, D.G., Van Dijk, A.I., McVicar, T.R., Adler, R.F., 2019. Mswep v2 global 3-hourly 0.1 precipitation: methodology and quantitative assessment. Bull. Am. Meteorol. Soc. 100 (3), 473–500.
- Bertoldi, G., Bozzoli, M., Crespi, A., Matiu, M., Giovannini, L., Zardi, D., Majone, B., 2023. Diverging snowfall trends across months and elevation in the northeastern italian alps. Int. J. Climatol. 43 (6), 2794–2819.
- Bhatt, B.C., Nakamura, K., 2005. Characteristics of monsoon rainfall around the himalayas revealed by trmm precipitation radar. Mon. Weather Rev. 133 (1), 149–165
- Boyle, D., 2001. Multicriteria Calibration of Hydrological Models. ph. d. thesis University of Arizona, Tucson, AZ, USA.
- Brandt, W.T., Bormann, K.J., Cannon, F., Deems, J.S., Painter, T.H., Steinhoff, D.F., Dozier, J., 2020. Quantifying the spatial variability of a snowstorm using differential airborne lidar. Water Resour. Res. 56 (3) e2019WR025331.
- Camici, S., Ciabatta, L., Massari, C., Brocca, L., 2018. How reliable are satellite precipitation estimates for driving hydrological models: a verification study over the mediterranean area. J. Hydrol. 563, 950–961.
- Cid, N., Bonada, N., Carlson, S.M., Grantham, T.E., Gasith, A., Resh, V.H., 2017. High variability is a defining component of mediterranean-climate rivers and their biota. Water 9 (1) 52
- Clark, M.P., Hendrikx, J., Slater, A.G., Kavetski, D., Anderson, B., Cullen, N.J., Kerr, T., Hreinsson, E.Ö., Woods, R.A., 2011. Representing spatial variability of snow water equivalent in hydrologic and land-surface models: a review. Water Resour. Res. 47 (7), W07539.
- Conde, V., Nico, G., Mateus, P., Catal\(\tilde{a}\)o, J., Kontu, A., Gritsevich, M., 2019. On the estimation of temporal changes of snow water equivalent by spaceborne sar interferometry: a new application for the sentinel-1 mission. J. Hydrol. Hydromech. 67, 93-100.
- De Lannoy, G.J., Reichle, R.H., Houser, P.R., Arsenault, K.R., Verhoest, N.E., Pauwels, V. R., 2010. Satellite-scale snow water equivalent assimilation into a high-resolution land surface model. J. Hydrometeorol. 11 (2), 352–369.
- Deschamps-Berger, C., Gascoin, S., Berthier, E., Deems, J., Gutmann, E., Dehecq, A., Shean, D., Dumont, M., 2020. Snow depth mapping from stereo satellite imagery in mountainous terrain: evaluation using airborne laser-scanning data. Cryosphere 14 (9), 2925–2940.
- Eberhart, R., Kennedy, J., 1995. Particle swarm optimization. In: Proceedings of the IEEE International Conference on Neural Networks, Vol. 4. Citeseer, pp. 1942–1948.

- Ebert, E.E., Janowiak, J.E., Kidd, C., 2007. Comparison of near-real-time precipitation estimates from satellite observations and numerical models. Bull. Am. Meteorol. Soc. 88 (1), 47–64.
- Formetta, G., Mantilla, R., Franceschi, S., Antonello, A., Rigon, R., 2011. The jgrass-newage system for forecasting and managing the hydrological budgets at the basin scale: models of flow generation and propagation/routing. Geosci. Model Dev. 4 (4), 943–955.
- Franz, K.J., Hogue, T.S., Sorooshian, S., 2008. Operational snow modeling: addressing the challenges of an energy balance model for national weather service forecasts. J. Hydrol. 360 (1–4), 48–66.
- Garen, D.C., Marks, D., 2005. Spatially distributed energy balance snowmelt modelling in a mountainous river basin: estimation of meteorological inputs and verification of model results. J. Hydrol. 315 (1–4), 126–153.
- Gelaro, R., McCarty, W., Suárez, M.J., Todling, R., Molod, A., Takacs, L., Randles, C.A., Darmenov, A., Bosilovich, M.G., Reichle, R., et al., 2017. The modern-era retrospective analysis for research and applications, version 2 (merra-2). J. Clim. 30 (14), 5419–5454.
- Germann, U., Galli, G., Boscacci, M., Bolliger, M., 2006. Radar precipitation measurement in a mountainous region. Q. J. R. Meteorol. Soc. 132 (618), 1669–1692.
- Girotto, M., Margulis, S.A., Durand, M., 2014. Probabilistic swe reanalysis as a generalization of deterministic swe reconstruction techniques. Hydrol. Process. 28 (12), 3875–3895.
- Girotto, M., Musselman, K.N., Essery, R.L., 2020. Data assimilation improves estimates of climate-sensitive seasonal snow. Curr. Clim. Change Rep. 6, 81–94.
- Günther, D., Marke, T., Essery, R., Strasser, U., 2019. Uncertainties in snowpack simulations—assessing the impact of model structure, parameter choice, and forcing data error on point-scale energy balance snow model performance. Water Resour. Res. 55 (4), 2779–2800.
- Gupta, H.V., Kling, H., Yilmaz, K.K., Martinez, G.F., 2009. Decomposition of the mean squared error and nse performance criteria: implications for improving hydrological modelling. J. Hydrol. 377 (1–2), 80–91.
- Hall, D.K., Riggs, G.A., Salomonson, V.V., DiGirolamo, N.E., Bayr, K.J., 2002. Modis snow-cover products. Remote Sens. Environ. 83 (1), 181–194.
- Han, P., Long, D., Li, X., Huang, Q., Dai, L., Sun, Z., 2021. A dual state-parameter updating scheme using the particle filter and high-spatial-resolution remotely sensed snow depths to improve snow simulation. J. Hydrol. 594, 125979.
- Harpold, A.A., Kaplan, M.L., Klos, P.Z., Link, T., McNamara, J.P., Rajagopal, S., Schumer, R., Steele, C.M., 2017. Rain or snow: hydrologic processes, observations, prediction, and research needs. Hydrol. Earth Syst. Sci. 21 (1), 1–22.
- He, M., Hogue, T.S., Franz, K.J., Margulis, S.A., Vrugt, J.A., 2011. Characterizing parameter sensitivity and uncertainty for a snow model across hydroclimatic regimes. Adv. Water Resour. 34 (1), 114–127.
- Hedrick, A.R., Marks, D., Havens, S., Robertson, M., Johnson, M., Sandusky, M., Marshall, H.-P., Kormos, P.R., Bormann, K.J., Painter, T.H., 2018. Direct insertion of nasa airborne snow observatory-derived snow depth time series into the isnobal energy balance snow model. Water Resour. Res. 54 (10), 8045–8063.
- Hersbach, H., Bell, B., Berrisford, P., Hirahara, S., Horányi, A., Muñoz-Sabater, J., Nicolas, J., Peubey, C., Radu, R., Schepers, D., et al., 2020. The era5 global reanalysis. Q. J. R. Meteorol. Soc. 146 (730), 1999–2049.
- Houle, E.S., Livneh, B., Kasprzyk, J.R., 2017. Exploring snow model parameter sensitivity using sobol'variance decomposition. Environ. Model Softw. 89, 144–158.
- Huffman, G.J., Bolvin, D.T., Braithwaite, D., Hsu, K., Joyce, R., Kidd, C., Nelkin, E.J., Sorooshian, S., Tan, J., Xie, P., 2018. Nasa global precipitation measurement (gpm) integrated multi-satellite retrievals for gpm (imerg). In: Algorithm Theoretical Basis Document (ATBD) Version 4.
- Immerzeel, W.W., Lutz, A.F., Andrade, M., Bahl, A., Biemans, H., Bolch, T., Hyde, S., Brumby, S., Davies, B., Elmore, A., et al., 2020. Importance and vulnerability of the world's water towers. Nature 577 (7790), 364–369.

- Jimeno-Sáez, P., Pulido-Velazquez, D., Collados-Lara, A.-J., Pardo-Igúzquiza, E., Senent-Aparicio, J., Baena-Ruiz, L., 2020. A preliminary assessment of the "undercatching" and the precipitation pattern in an alpine basin. Water 12 (4), 1061.
- Kang, D., Lee, K., Kim, E., 2021. Improving cold-region streamflow estimation by winter precipitation adjustment using passive microwave snow remote sensing datasets. Environ. Res. Lett. 16 (4), 044055.
- Karbou, F., Veyssière, G., Coleou, C., Dufour, A., Gouttevin, I., Durand, P., Gascoin, S., Grizonnet, M., 2021. Monitoring wet snow over an alpine region using sentinel-1 observations. Remote Sens. 13 (3), 381.
- Leinss, S., Parrella, G., Hajnsek, I., 2014. Snow height determination by polarimetric phase differences in x-band sar data. IEEE J. Sel. Top. Appl. Earth Obs. Remote Sens. 7 (9), 3794–3810.
- Lievens, H., Demuzere, M., Marshall, H.-P., Reichle, R.H., Brucker, L., Brangers, I., de Rosnay, P., Dumont, M., Girotto, M., Immerzeel, W.W., et al., 2019. Snow depth variability in the northern hemisphere mountains observed from space. Nat. Commun. 10 (1), 4629.
- Lievens, H., Brangers, I., Marshall, H.-P., Jonas, T., Olefs, M., De Lannoy, G., 2022.
  Sentinel-1 snow depth retrieval at sub-kilometer resolution over the european alps.
  Cryosphere 16 (1), 159–177.
- Liu, X., Zhang, M., Wang, S., Wang, J., Zhao, P., Zhou, P., 2017. Assessment of diurnal variation of summer precipitation over the qilian mountains based on an hourly merged dataset from 2008 to 2014. J. Geogr. Sci. 27, 326–336.
- Lundberg, A., Koivusalo, H., 2003. Estimating winter evaporation in boreal forests with operational snow course data. Hydrol. Process. 17 (8), 1479–1493.
- Lundquist, J., Hughes, M., Gutmann, E., Kapnick, S., 2019. Our skill in modeling mountain rain and snow is bypassing the skill of our observational networks. Bull. Am. Meteorol. Soc. 100 (12), 2473–2490.
- Lundquist, J.D., Minder, J.R., Neiman, P.J., Sukovich, E., 2010. Relationships between barrier jet heights, orographic precipitation gradients, and streamflow in the northern sierra nevada. J. Hydrometeorol. 11 (5), 1141–1156.
- Maggioni, V., Nikolopoulos, E.I., Anagnostou, E.N., Borga, M., 2017. Modeling satellite precipitation errors over mountainous terrain: the influence of gauge density, seasonality, and temporal resolution. IEEE Trans. Geosci. Remote Sens. 55 (7), 4130–4140.
- Magnusson, J., Winstral, A., Stordal, A.S., Essery, R., Jonas, T., 2017. Improving physically based snow simulations by assimilating snow depths using the particle filter. Water Resour. Res. 53 (2), 1125–1143.
- Margulis, S.A., Girotto, M., Cortés, G., Durand, M., 2015. A particle batch smoother approach to snow water equivalent estimation. J. Hydrometeorol. 16 (4), 1752–1772.
- Margulis, S.A., Fang, Y., Li, D., Lettenmaier, D.P., Andreadis, K., 2019. The utility of infrequent snow depth images for deriving continuous space-time estimates of seasonal snow water equivalent. Geophys. Res. Lett. 46 (10), 5331–5340.
- Marin, C., Bertoldi, G., Premier, V., Callegari, M., Brida, C., Hürkamp, K., Tschiersch, J., Zebisch, M., Notarnicola, C., 2020. Use of sentinel-1 radar observations to evaluate snowmelt dynamics in alpine regions. Cryosphere 14 (3), 935–956.
- Marks, D., Domingo, J., Susong, D., Link, T., Garen, D., 1999. A spatially distributed energy balance snowmelt model for application in mountain basins. Hydrol. Process. 13 (12–13), 1935–1959.
- Matiu, M., Crespi, A., Bertoldi, G., Carmagnola, C.M., Marty, C., Morin, S., Schöner, W., Cat Berro, D., Chiogna, G., De Gregorio, L., et al., 2020. Observed snow depth trends in the european alps 1971 to 2019. Cryosphere Discuss. 2020, 1–50.
- Mei, Y., Nikolopoulos, E.I., Anagnostou, E.N., Zoccatelli, D., Borga, M., 2016. Error analysis of satellite precipitation-driven modeling of flood events in complex alpine terrain. Remote Sens. 8 (4), 293.
- Moore, R., 1985. The probability-distributed principle and runoff production at point and basin scales. Hydrol. Sci. J. 30 (2), 273–297.
- Mott, R., Scipión, D., Schneebeli, M., Dawes, N., Berne, A., Lehning, M., 2014. Orographic effects on snow deposition patterns in mountainous terrain. J. Geophys. Res. Atmos. 119 (3), 1419–1439.
- Mott, R., Vionnet, V., Grünewald, T., 2018. The seasonal snow cover dynamics: review on wind-driven coupling processes. Front. Earth Sci. 6, 197.
- Mott, R., Winstral, A., Cluzet, B., Helbig, N., Magnusson, J., Mazzotti, G., Quéno, L., Schirmer, M., Webster, C., Jonas, T., 2023. Operational snow-hydrological modeling for Switzerland. Front. Earth Sci. 11, 1228158.
- Pagano, T., Garen, D., Sorooshian, S., 2004. Evaluation of official western us seasonal water supply outlooks, 1922–2002. J. Hydrometeorol. 5 (5), 896–909.
- Painter, T.H., Berisford, D.F., Boardman, J.W., Bormann, K.J., Deems, J.S., Gehrke, F., Hedrick, A., Joyce, M., Laidlaw, R., Marks, D., et al., 2016. The airborne snow observatory: fusion of scanning lidar, imaging spectrometer, and physically-based

- modeling for mapping snow water equivalent and snow albedo. Remote Sens. Environ. 184, 139–152.
- Prein, A.F., Gobiet, A., 2017. Impacts of uncertainties in european gridded precipitation observations on regional climate analysis. Int. J. Climatol. 37 (1), 305–327.
- Qi, W., Zhang, C., Fu, G., Sweetapple, C., Zhou, H., 2016. Evaluation of global fineresolution precipitation products and their uncertainty quantification in ensemble discharge simulations. Hydrol. Earth Syst. Sci. 20 (2), 903–920.
- Qin, Y., Abatzoglou, J.T., Siebert, S., Huning, L.S., AghaKouchak, A., Mankin, J.S., Hong, C., Tong, D., Davis, S.J., Mueller, N.D., 2020. Agricultural risks from changing snowmelt. Nat. Clim. Chang. 10 (5), 459–465.
- Raleigh, M., Lundquist, J., Clark, M., 2015. Exploring the impact of forcing error characteristics on physically based snow simulations within a global sensitivity analysis framework. Hydrol. Earth Syst. Sci. 19 (7), 3153–3179.
- Rasmussen, R., Baker, B., Kochendorfer, J., Meyers, T., Landolt, S., Fischer, A.P., Black, J., Thériault, J.M., Kucera, P., Gochis, D., et al., 2012. How well are we measuring snow: the noaa/faa/ncar winter precipitation test bed. Bull. Am. Meteorol. Soc. 93 (6), 811–829.
- Rice, R., Bales, R.C., 2010. Embedded-sensor network design for snow cover measurements around snow pillow and snow course sites in the Sierra Nevada of California. Water Resour. Res. 46 (3).
- Sarmadi, F., Huang, Y., Thompson, G., Siems, S.T., Manton, M.J., 2019. Simulations of orographic precipitation in the snowy mountains of southeastern Australia. Atmos. Res. 219, 183–199.
- Scheel, M., Rohrer, M., Huggel, C., Santos Villar, D., Silvestre, E., Huffman, G., 2011. Evaluation of trmm multi-satellite precipitation analysis (tmpa) performance in the Central Andes region and its dependency on spatial and temporal resolution. Hydrol. Earth Syst. Sci. 15 (8), 2649–2663.
- Skaugen, T., Stranden, H.B., Saloranta, T., 2012. Trends in snow water equivalent in Norway (1931–2009). Hydrol. Res. 43 (4), 489–499.
- Smyth, E.J., Raleigh, M.S., Small, E.E., 2022. The challenges of simulating swe beneath forest canopies are reduced by data assimilation of snow depth. Water Resour. Res. 58 (3) e2021WR030563.
- Speirs, P., Gabella, M., Berne, A., 2017. A comparison between the gpm dual-frequency precipitation radar and ground-based radar precipitation rate estimates in the swiss alps and plateau. J. Hydrometeorol. 18 (5), 1247–1269.
- Tsang, L., Durand, M., Derksen, C., Barros, A.P., Kang, D.-H., Lievens, H., Marshall, H.-P., Zhu, J., Johnson, J., King, J., et al., 2022. Global monitoring of snow water equivalent using high-frequency radar remote sensing. Cryosphere 16 (9), 3531–3573.
- Van Leeuwen, P.J., 2009. Particle filtering in geophysical systems. Mon. Weather Rev. 137 (12), 4089–4114.
- Viviroli, D., Dürr, H.H., Messerli, B., Meybeck, M., Weingartner, R., 2007. Mountains of the world, water towers for humanity: typology, mapping, and global significance. Water Resour. Res. 43 (7).
- Vrugt, J.A., Gupta, H.V., Bouten, W., Sorooshian, S., 2003. A shuffled complex evolution metropolis algorithm for optimization and uncertainty assessment of hydrologic model parameters. Water Resour. Res. 39 (8).
- Wagener, T., Boyle, D.P., Lees, M.J., Wheater, H.S., Gupta, H.V., Sorooshian, S., 2001.

  A framework for development and application of hydrological models. Hydrol. Earth Syst. Sci. 5 (1), 13–26.
- Wang, S., Liu, J., Wang, J., Qiao, X., Zhang, J., 2019. Evaluation of gpm imerg v05b and trmm 3b42v7 precipitation products over high mountainous tributaries in Lhasa with dense rain gauges. Remote Sens. 11 (18), 2080.
- Winstral, A., Magnusson, J., Schirmer, M., Jonas, T., 2019. The bias-detecting ensemble: a new and efficient technique for dynamically incorporating observations into physics-based, multilayer snow models. Water Resour. Res. 55 (1), 613–631.
- Wrzesien, M.L., Pavelsky, T.M., Durand, M.T., Dozier, J., Lundquist, J.D., 2019. Characterizing biases in mountain snow accumulation from global data sets. Water Resour. Res. 55 (11), 9873–9891.
- Xu, R., Tian, F., Yang, L., Hu, H., Lu, H., Hou, A., 2017. Ground validation of gpm imerg and trmm 3b42v7 rainfall products over southern tibetan plateau based on a highdensity rain gauge network. J. Geophys. Res. Atmos. 122 (2), 910–924.
- Xue, Y., Houser, P.R., Maggioni, V., Mei, Y., Kumar, S.V., Yoon, Y., 2021. Evaluation of high mountain asia-land data assimilation system (version 1) from 2003 to 2016, part i: a hyper-resolution terrestrial modeling system. J. Geophys. Res. Atmos. 126 (8) e2020JD034131.
- Zaramella, M., Borga, M., Zoccatelli, D., Carturan, L., 2019. Topmelt 1.0: a topography-based distribution function approach to snowmelt simulation for hydrological modelling at basin scale. Geosci. Model Dev. 12 (12), 5251–5265.